

Characterization of atomic step structures on CaF₂(111) by their electric potential

H. H. Pieper,¹ C. Barth,^{2,a)} and M. Reichling^{1,a)}

¹Fachbereich Physik, Universität Osnabrück, Barbarastr. 7, 49076 Osnabrück, Germany

²CINaM-CNRS UPR 3118, Campus de Luminy, Case 913, 13288 Marseille Cedex 09, France

(Received 5 April 2012; accepted 16 July 2012; published online 30 July 2012)

The structure and polarity of step edges on cleaved CaF₂(111) are investigated by non-contact atomic force microscopy (NC-AFM) and Kelvin probe force microscopy. Ledges produced by cleaving the crystal appear with two distinctly different polarities denoted as type I and type II arising from the sectioning of ledges with steps having different polarities. With respect to the stoichiometric terrace, the surface potential is slightly reduced at ledges predominately composed of type I steps, while the potential of ledges predominantly composed of type II steps is significantly higher (typically 100 mV). We propose that the positive potential of type II steps stems from low coordinated Ca²⁺ ions inducing a dipole at step edges and confirm this by atomically resolved NC-AFM images revealing the Ca²⁺ ion sub-lattice with repulsive-mode imaging contrast. © 2012 American Institute of Physics. [<http://dx.doi.org/10.1063/1.4739944>]

Ionic materials are of importance in microelectronics as they can be used as electrically insulating layers in devices like, for instance, MgO as a giant magnetic resistance material in a tunnel junction.^{1,2} Besides oxides, CaF₂ (fluorite) as a strongly ionic compound and excellent electrical insulator, has been introduced as an electronic material for tunnel junctions,³ field effect transistors,⁴ phototransistors,⁵ and electroluminescent devices.⁶ Fluorite is well suited for electronics applications as by epitaxial growth on Si(111) and Si(001) surfaces, it can well be integrated into conventional microelectronics technology,⁷ although, there are limitations as fluorite is susceptible to electron induced degradation.^{8,9} For the practical use of insulating ionic materials, the knowledge of surface properties like the local electrostatic surface potential is of great importance as, for instance, surface step structures often contain charged defects,^{10,11} which strongly influence the local surface potential.¹²

Here, we investigate ledges and specifically their surface potential on CaF₂(111) surfaces prepared by cleaving in the ultra-high vacuum (UHV). By high resolution non-contact atomic force microscopy (NC-AFM) imaging,^{13,14} we reveal that ledges formed by cleaving can be decomposed in a series of steps with distinctly different character, namely type I and type II steps where, depending on the ledge direction, one of the step types may dominate. By Kelvin probe force microscopy (KPFM),¹⁵ we demonstrate that the electrostatic potential at ledges predominantly formed of type II step edges is about 100 mV higher than the potential of ledges predominantly formed by type I steps. Cleaving produces non-equilibrium step structures composed of ledges mostly forming acute angles with each other.¹⁶ This is in contrast to the surface preparation of fluorite type crystals where annealing to high temperature^{17–20} creates a thermodynamic equilibrium morphology dominated by hexagonal structures with step edges parallel to $\langle\bar{1}10\rangle$ surface directions. Below, we demonstrate, however, that the ledges found on cleaved

surfaces are composed of sections of $\langle\bar{1}10\rangle$ steps (see discussion of results shown in Fig. 5) and, therefore, we start here with a discussion of the atomic structure of such steps in very detail by the model presented in Fig. 1. This is a schematic representation of a fluorite island with a height of one F-Ca-F triple layer drawn as an epitaxial continuation of the underneath CaF₂(111) surface. Due to the stacking of (111) planes in fluorite, the triple layer of the island and the triple layer of the surface exhibit the same orientation, but equivalent ions are shifted laterally along $[\bar{2}11]$ by $x = a_{\text{CaF}_2}/\sqrt{6} = 223$ pm, where a_{CaF_2} is the CaF₂ lattice constant. The regularly shaped island has step edges parallel to $\langle\bar{1}10\rangle$ directions. Two adjacent steps include an angle of 120° and have alternating type I and type II character as labeled by black and white arrows, respectively. The existence of two different kinds of step edges is a result of the three-fold symmetry of the (111) surface of fluorite. When crossing a step perpendicular to a step edge, the direction of descent from the island to the surface determines the step character. Descending a step in $[\bar{2}11]$, $[1\bar{2}1]$, or $[11\bar{2}]$ direction implies type I character while descending a step in the opposite directions, namely $[2\bar{1}\bar{1}]$, $[\bar{1}2\bar{1}]$, or $[\bar{1}\bar{1}2]$ implies a type II step. As a consequence, two steps belonging to one island are always of opposite type if they are adjacent or if they are parallel to each other. Type I and type II steps can also be characterized by their facets: type I steps predominantly form neutral {110} and {111} facets^{21,22} while type II steps predominantly form polar {001} facets as indicated by the dotted lines in Fig. 1(b).²¹

Experiments are performed in a UHV system operated at a base pressure in the low 10⁻¹⁰ mbar range with a commercial room temperature AFM/STM system (Omicron NanoTechnology GmbH, Taunusstein, Germany). Silicon cantilevers (p-doped, 0.015 Ωcm specific resistance) with an eigenfrequency of about 275 kHz and a stiffness of about 30 N/m (Type NCH, Nanoworld AG, Neuchâtel, Switzerland) are used for atomic resolution NC-AFM studies while KPFM measurements, which are done simultaneously to

^{a)}Electronic addresses: barth@cinam.univ-mrs.fr and reichling@uos.de.

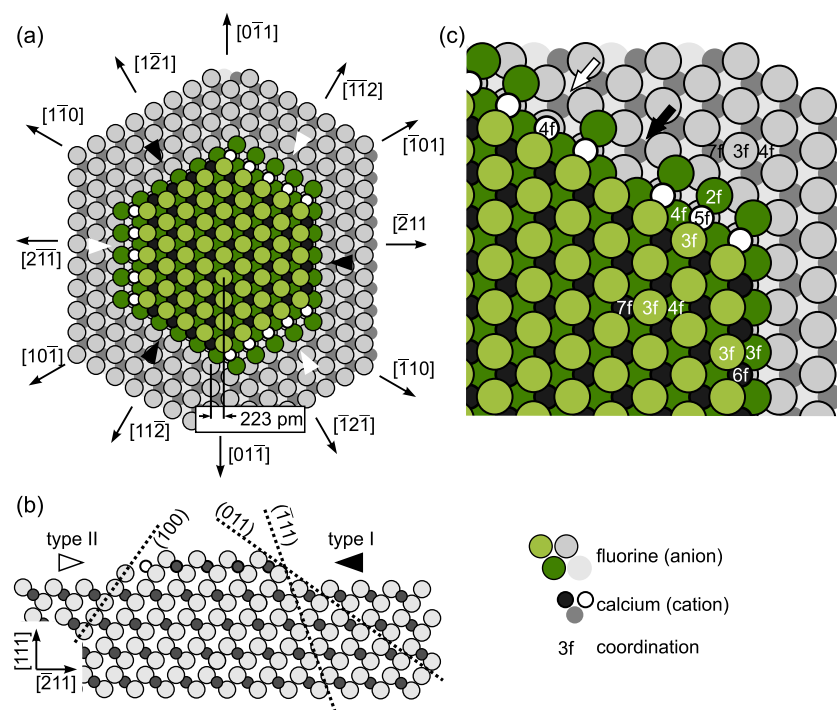


FIG. 1. Model of an island on the CaF_2 (111) surface in top view (a) and side view (b) with main crystallographic directions. Type I and type II steps are labeled by black and white arrows, respectively. The magnification (c) includes a positively charged F^- and a negatively charged Ca^{2+}F^- vacancy (white and black arrows) at a type II step edge.

lower resolution NC-AFM imaging, are performed with cantilevers having an eigenfrequency of about 74 kHz and a stiffness of about 3 N/m (Type FM, Nanoworld AG, Neuchâtel, Switzerland). Cantilevers are Ar^+ ion-sputtered prior to their use in experiments to remove tip contamination. KPFM measurements are performed in the frequency modulation mode,²³ where the bias voltage is the sum of a DC voltage V_{DC} and a sinusoidally modulated voltage with an amplitude of $V_{\text{AC}} = 1.5$ V (modulation frequency $f_{\text{AC}} = 474$ Hz). During imaging, the electrostatic tip-surface interaction is minimized by a feedback loop regulating V_{DC} to obtain zero force for the first harmonic at f_{AC} as measured by a lock-in detector. KPFM images display the inverted value of the regulated voltage V_{DC} applied between the tip and the electrically conducting sample support plate. A descriptive interpretation of KPFM contrast formation and its relation to the surface potential on the insulating crystal is given in the supporting information.²⁴ Surface preparation comprises cleaning the crystal by annealing at 880 K in UHV and cleaving the crystal along the (111) plane after cooling to room temperature with a device described in detail elsewhere.²⁵ Subsequently, the crystal is annealed at a temperature of 460 K to remove excess surface charge and is transferred to the force microscopy system.

Figure 2(a) shows the typical nanometer scale surface topography as obtained with NC-AFM while Fig. 2(b) represents the simultaneously recorded KPFM image. The cross-sectional analysis shown in Fig. 2(c) reveals that the surface morphology is dominated by atomically flat terraces separated by steps with a F-Ca-F triple-layer height of $h_{\text{TL}} = a_{\text{CaF}_2} / \sqrt{3} = 315$ pm or an integer multiple of this height. As seen in Fig. 2(a), cleaving produces ledges enclosing angles of typically 30° to 45° with each other. Many of them are aligned parallel to $[10\bar{1}]$ which is a member of the family of preferred direction of steps on fluorite (see Fig. 1).¹⁷ A striking observation in the topography image is the bright appearance of ledges (see also cross-section in

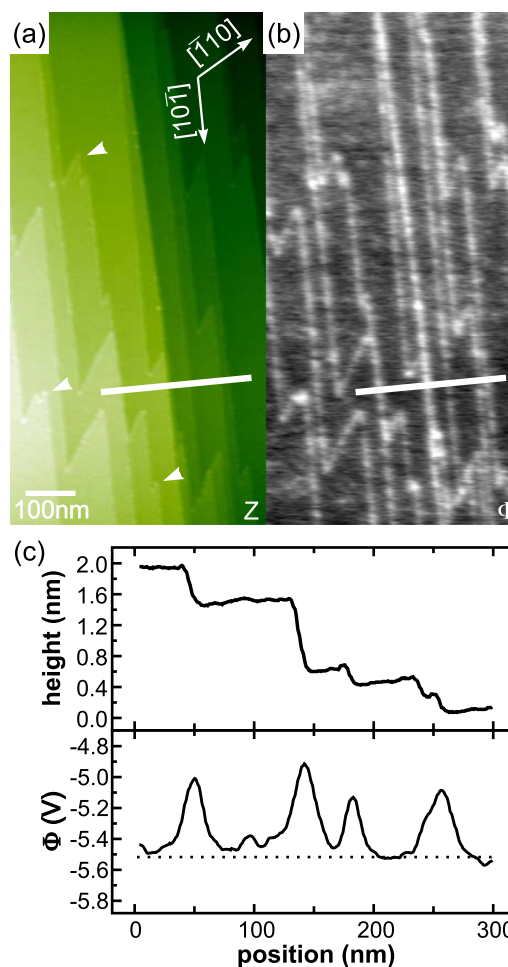


FIG. 2. NC-AFM image (a) and simultaneously recorded KPFM image (b) of ledges on the CaF_2 (111) surface. The white arrows in frame (a) indicate kink sites exhibiting an enhanced surface potential contrast. The line profile (c) reveals step edges with a height corresponding to one or two F-Ca-F triple layers and shows the corresponding KPFM contrast variations.

Fig. 2(c)) and even more pronounced bright kinks (see arrows in Fig. 2(a)). In accordance with earlier observations, we find that the contrast enhancement of ledges and kinks is a small artifact in images like the ones shown here but the effect is very pronounced when the KPFM compensation is not activated during topography imaging.²⁶ This points to electrostatic interactions being the origin of the contrast enhancement what is confirmed by simultaneously taken KPFM images as the one shown in Fig. 2(b). Ledges appear bright what implies a more positive potential than present on the terraces, which are perfectly stoichiometric, neutral, and free of dipoles.²⁴ Important to note is the discrete nature of the charging, namely, the bright contrast at ledges is not homogeneous but appears as a chain of more or less pronounced spots while it is specifically strong at kink sites (see arrows in Fig. 2(a)). Presumably, this stems from a local variation of the potential determined by the atomic scale substructure of the ledges.

Figure 3 shows ledges after cleaving and heating the same crystal a second time. As a result of different cleaving conditions, the ledges now have a certain inclination with respect to the $[\bar{1}10]$ direction, as determined from images with atomic resolution (see below). The analysis of the step structure demonstrates that the charging behavior strongly depends on the orientation of the ledge in the surface plane. The zigzag lines in black and white shown in Fig. 3(a) are a schematic representation of the decomposition of the ledges enclosing one of the terraces into sections of type I steps (black lines and black arrows) and type II steps (white lines and white arrow). Note that the sectioning is schematically shown on a much larger length scale to visualize that the left ledge is a type I ledge, i.e., predominantly composed of type I steps while the right ledge is a type II ledge, i.e., predominantly composed of type II steps. However, the true sectioning is due to type I and II steps having an average length smaller than the lateral resolution of NC-AFM images taken

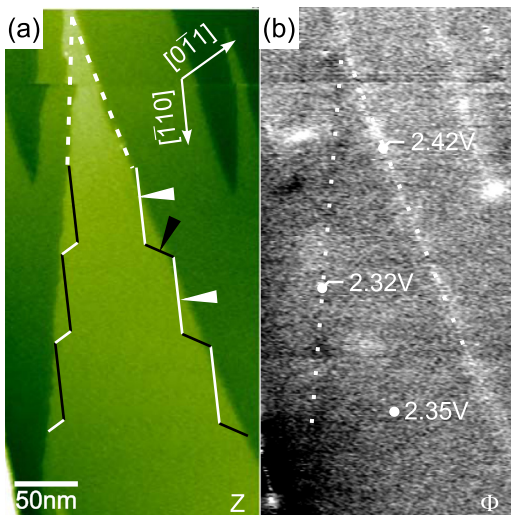


FIG. 3. NC-AFM image (a) and simultaneously recorded KPFM image (b) of a step structure composed of type I and type II ledges. The sectioning in type I and type II regions is schematically depicted by black and white sections and arrows according to the model introduced in Fig. 1. Note that the sectioning is drawn here out of scale to demonstrate that the left ledge is predominantly composed of type I steps while the right ledge is predominantly composed of type II steps.

at this scale. The striking observation is that type I ledges do not exhibit a bright contrast in the KPFM image but have a slightly more negative potential than the terrace. On the contrary, type II ledges appear bright corresponding to a KPFM potential difference of 70 mV with respect to the neutral terraces. Performing the same type of decomposition of the ledges in Fig. 2 reveals that all of them are exclusively or predominantly composed of type II steps consistently explaining their continuous bright appearance.

The key to understanding the potential of step edges is a detailed analysis of the atomic structures of type I and II steps. The structures of both types of steps are schematically depicted in Fig. 4 in a top view (a) and in a side view (b) perpendicular to the surface along the $[\bar{1}\bar{1}2]$ direction. Type II steps are shown in two possible configurations where model IIa represents a stoichiometric step while model IIb represents a non-stoichiometric step with the lower row of 2-fold fluorine ions along the step edge missing. The schematic ball model shown in Fig. 4(a) is superimposed to the result of a NC-AFM measurement exhibiting atomic corrugation and is drawn as a virtual F-Ca-F triple-layer on top of the surface, i.e., as an epitaxial continuation with the stacking of the fluorite crystal. An unambiguous assignment of surface directions for this and all other images taken on the same crystal is possible as the atomically resolved NC-AFM image reveals typical features of the triangular contrast (highlighted by the white bordered triangles in Fig. 4(a)) that identifies all atomic positions in the topmost F-Ca-F triple-layer of the (111) surface.^{27,28}

In KPFM imaging, type I steps hardly exhibit any contrast. This is in accordance with the fact, that they form $\{111\}$ facets with the same arrangement of ions as the (111) terraces. The slight dark contrast, however, points to a net negative potential that presumably stems from additional

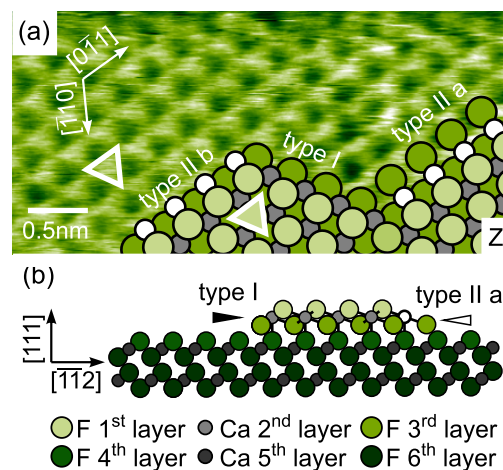


FIG. 4. (a) Model of a F-Ca-F triple layer island with type I and type II step edges superimposed to an atomically resolved topography image obtained with a positively terminated tip. The triangular shape image contrast (enhanced by white triangles at two ion sites) unambiguously defines the directions in the surface plane (see Refs. 27 and 28). To yield the regular hexagonal surface pattern, the NC-AFM image has been corrected for thermal drift. The small white circles in the model mark the outermost row of 5-fold coordinated Ca^{2+} ions which is either coordinated to a lower row of 2-fold coordinated F^- ions (type IIa step) or not (type IIb step). (b) Side view on the model step structure visualizing the coordination of ions (indicated by small black lines).

fluorine ions at kink positions. To explain this, we recall that in the bulk of fluorite, anti-Frenkel-disorder is the dominant mechanism for intrinsic defect creation.²⁹ Even at room temperature, a small but finite number of F^- ions on interstitial positions is present in the crystal where the charge of these ions is compensated by anion vacancy defects.³⁰ For the (111) surface, it has been predicted that fluorine ions located at type I step or kink positions are energetically favored by 1.52 and 2.25 eV compared to fluorine ions on interstitial sites.³¹ Therefore, interstitial-vacancy pairs in the near surface region form a Frenkel-Debye boundary layer where fluorine ions are located at step edges and kink sites while positive vacancies remain below the surface. However, the effective polarization is very small as a simulation predicts³¹ only about 10 fluorine ions per μm^2 what is in qualitative agreement with our experimental findings where {111} facets hardly show any but a dark contrast.

The edge forming Ca^{2+} ions of a stoichiometric step (type IIa) are low coordinated as they have only 5 next neighbor fluorine ions in comparison to the 7 neighbors for a Ca^{2+} ion in the terrace (see Figs. 1(c) and 4(a)). We assume here that the last step forming row of fluorines is located below the latter Ca^{2+} ions in the third layer of the F-Ca-F triple-layer as it has been proposed earlier.¹⁷ We further propose that the step forming Ca^{2+} ions are the key to the positive potential found at type II step edges. As they protrude from the step edge and their charge is only compensated by adjacent F^- ions mostly located in the 3rd layer, a dipole is formed with its positive end pointing out of the step edge. The contrast in KPFM is a result of the row of such dipoles providing a positive surface potential, although, type IIa steps are stoichiometric. Note that the number of protruding Ca^{2+} ions and, hence, the dipole strength increases with step height explaining that a stronger KPFM contrast is observed for higher ledges.

Worth mentioning are the 2-fold coordinated fluorine ions in front of the type II steps: Due to their very low coordination (2-fold) their removal is facilitated, especially during the cleavage process. A complete clearance of these fluorines results in a non-stoichiometric step with a strong positive charge as represented by the model type IIb shown in Figs. 4 and 1(c). Such a high positive charge at a step needs to be compensated, which can be principally accomplished by fluorine interstitials below the surface forming a Frenkel-Debye layer with a dipole orientation opposite to the one described above. We anticipate, however, that the non-stoichiometry of IIb steps is restricted to a few individual step or kink sites only since we generally observe small surface potential differences of around 100 mV.

In quest of evidence for the presence of low-coordinated Ca^{2+} ions at type II steps, we perform atomically resolved NC-AFM imaging right at a step edge applying an imaging mode enhancing the cation lattice.²⁸ To obtain the respective results shown in Fig. 5(a), scanning is performed in a quasi-constant height manner by choosing a very slow topography feedback loop.¹⁹ When adjusting the tip-surface distance to a very small value, the cation lattice appears with a strong contrast of dark circular spots, which clearly identifies the Ca^{2+} lattice positions on a bright background formed by the anion sub-lattices. The dark spots result from a repulsive interaction of a positively terminated tip with the cations.^{27,28} The

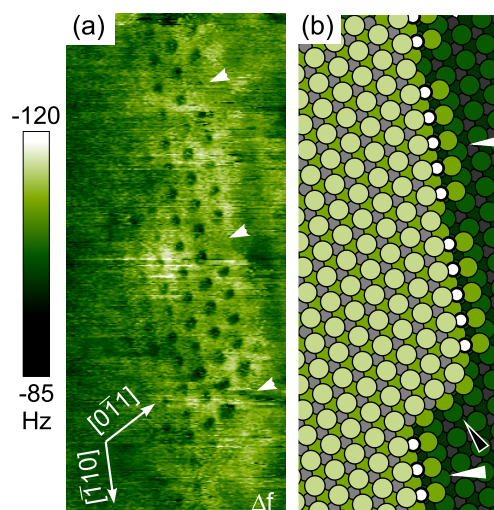


FIG. 5. (a) Quasi-constant height NC-AFM image of a step structure revealing the Ca^{2+} sub-lattice as dark spots. Missing Ca^{2+} ions are tagged by white arrows. (b) Model of the step structure from frame (a). The color code to denote ions is the same as the one introduced in Figs. 1 and 4.

contrast effect is enhanced by the imaging plane being slightly tilted with respect to the surface plane so that the described imaging conditions are present only at the ledge and in a small adjacent stripe on the upper terrace. This image yields direct atomic scale evidence that the investigated cleavage ledge is composed of straight segments parallel to $\langle 110 \rangle$ directions. The corresponding decomposition in type I and type II segments is illustrated in the model of the step structure shown in Fig. 5(b). While the apparent lattice is overall regular and rather perfect, single vacancy defects marked by arrows in Fig. 5(a) appear right at the step edge. As illustrated in Figs. 5(b) and 1(c), we propose that they are missing pairs of 5-fold coordinated Ca^{2+} and 2-fold coordinated F^- ions in the bordering row, a feature resulting in a negative local charge at the defective sites. The occurrence of such cation vacancies together with the presence of type I sections can explain that the otherwise uniformly bright KPFM contrast of type II ledges is found to be interrupted by dark sections as it is seen, for instance, in Figs. 2(b) and 3(b). Note that removing a protruding Ca^{2+} ion from a type II step costs much less energy than the formation of a cation vacancy in the bulk or on a terrace³² due to the lower coordination of the Ca^{2+} ion at the step.

Within the presented model, we can explain all of our experimental findings. The neutrality or slightly negative potential found at type I ledges is due to the compact structure of this type of step edge and a small amount of attached fluorine ions compensated by the formation of a Frenkel-Debye layer in the vicinity of the step edge. The positive potential found at type II ledges is due to dipoles formed by exposed and low coordinated Ca^{2+} ions whereas the apparent inhomogeneity of type II ledges is caused either by the nanoscale sectioning into type I and type II regions or by $\text{Ca}^{2+}F^-$ defects. This model describes the situation of a stepped surface that is overall stoichiometric and neutral with individual local charges compensated locally by the Frenkel-Debye mechanism. Note that this has to be

discriminated from the situation, which can be found on a freshly cleaved surface not subjected to annealing. Experience from a large number of cleavage experiments shows that a fluorite surface may be overall positively or negatively charged right after cleavage of the crystal. In this case, the applied bias voltage varies from values of a few volts to more than 100 V depending on the cleaving conditions that are to a large extent unpredictable and uncontrollable. This charge may be preserved over very long periods (days or weeks) or may decay rapidly, specifically when the ionic conductivity is increased by heating the crystal.^{15,25} In contrast, for a perfectly cleaved surface, on which atomically flat terraces extending over many μm^2 can be found, the overall surface potential is virtually zero right after cleaving (no annealing). This clearly points to the key role ledges play for the surface potential of cleaved fluorite. Here, we have shown that for the relaxed situation, the nanoscale composition of cleavage ledges from different types of step edges is consistently reflected in variations of the local surface potential found at step edges and kink sites.

Stimulating discussions with Claude R. Henry and Philipp Rahe are gratefully acknowledged. This work has been supported by the COST Action CM1104.

- ¹S. S. P. Parkin, C. Kaiser, A. Panchula, P. M. Rice, B. Hughes, M. Samant, and S. H. Yang, *Nature Mater.* **3**, 862 (2004).
- ²S. Yuasa, T. Nagahama, A. Fukushima, Y. Suzuki, and K. Ando, *Nature Mater.* **3**, 868 (2004).
- ³T. Harianto, K. Kobayashi, T. Suemasu, and H. Akinaga, *Jpn. J. Appl. Phys. Part 2* **46**, L904 (2007).
- ⁴Y. Y. Illarionov, M. I. Vexler, S. M. Sutorin, V. V. Fedorov, and N. S. Sokolov, *Tech. Phys. Lett.* **36**, 404 (2010).
- ⁵M. I. Vexler, Y. Y. Illarionov, S. M. Sutorin, V. V. Fedorov, and N. S. Sokolov, *Semicond. Sci. Technol.* **25**, 095007 (2010).
- ⁶K. Jinen, T. Kikuchi, M. Watanabe, and M. Asada, *Jpn. J. Appl. Phys. Part 1* **45**, 3656 (2006).

- ⁷M. I. Vexler, N. S. Sokolov, I. V. Grekhov, S. Ikeda, A. K. Kaveev, A. V. Krupin, K. Saiki, K. Tsutsui, and S. E. Tyaginov, *Microelectron. Eng.* **84**, 2247 (2007).
- ⁸M. Reichling, R. M. Wilson, R. Bennewitz, R. T. Williams, S. Gogoll, E. Stenzel, and E. Matthias, *Surf. Sci.* **366**, 531 (1996).
- ⁹R. Bennewitz, D. Smith, and M. Reichling, *Phys. Rev. B* **59**, 8237 (1999).
- ¹⁰C. Barth and C. R. Henry, *Appl. Phys. Lett.* **89**, 252119 (2006).
- ¹¹C. Barth and C. R. Henry, *J. Phys. Chem. C* **113**, 247 (2009).
- ¹²C. Barth and C. R. Henry, *Phys. Rev. Lett.* **98**, 136804 (2007).
- ¹³J. V. Lauritsen and M. Reichling, *J. Phys.: Condens. Matter* **22**, 263001 (2010).
- ¹⁴C. Barth, A. S. Foster, C. R. Henry, and A. L. Shluger, *Adv. Mater.* **23**, 477 (2011).
- ¹⁵C. Barth and C. R. Henry, *Nanotechnology* **17**, 155 (2006).
- ¹⁶L. Tröger, J. Schütte, F. Ostendorf, A. Kühnle, and M. Reichling, *Rev. Sci. Instrum.* **80**, 063703 (2009).
- ¹⁷J. B. Engelhardt, H. Dabringhaus, and K. Wandelt, *Surf. Sci.* **448**, 187 (2000).
- ¹⁸M. Schick, H. Dabringhaus, and K. Wandelt, *Surf. Sci.* **592**, 42 (2005).
- ¹⁹S. Gritschneder, Y. Namai, Y. Iwasawa, and M. Reichling, *Nanotechnology* **16**, S41 (2005).
- ²⁰S. Torbrügge, M. Cranney, and M. Reichling, *Appl. Phys. Lett.* **93**, 073112 (2008).
- ²¹V. E. Puchin, A. V. Puchina, M. Huisinga, and M. Reichling, *J. Phys.: Condens. Matter* **13**, 2081 (2001).
- ²²M. Schick, H. Dabringhaus, and K. Wandelt, *J. Phys.: Condens. Matter* **16**, L33 (2004).
- ²³U. Zerweck, C. Loppacher, T. Otto, S. Grafström, and L. M. Eng, *Phys. Rev. B* **71**, 125424 (2005).
- ²⁴See supplementary material at <http://dx.doi.org/10.1063/1.4739944> for a model for KPFM contrast formation.
- ²⁵C. Barth, C. Claeyss, and C. R. Henry, *Rev. Sci. Instrum.* **76**, 083907 (2005).
- ²⁶T. Arai, S. Gritschneder, L. Tröger, and M. Reichling, *J. Vac. Sci. Technol. B* **28**, 1279 (2010).
- ²⁷A. S. Foster, C. Barth, A. L. Shluger, and M. Reichling, *Phys. Rev. Lett.* **86**, 2373 (2001).
- ²⁸C. Barth, A. S. Foster, M. Reichling, and A. L. Shluger, *J. Phys.: Condens. Matter* **13**, 2061 (2001).
- ²⁹W. Hayes and A. M. Stoneham, *Defects and Defect Processes in Nonmetallic Solids* (Wiley-Interscience Publication, New York, 1985).
- ³⁰A. S. Foster, T. Trevethan, and A. L. Shluger, *Phys. Rev. B* **80**, 115421 (2009).
- ³¹H. Dabringhaus and M. F. Butman, *J. Phys.: Condens. Matter* **15**, 5801 (2003).
- ³²C. R. A. Catlow, M. J. Norgett, and T. A. Ross, *J. Phys. C* **10**, 1627 (1977).